Oscillating-grid experiments in water and superfluid helium

Rose E. Honey, Robert Hershberger, and Russell J. Donnelly*
Department of Physics, University of Oregon, Eugene, Oregon 97403, USA

Diogo Bolster
Department of Civil Engineering and Geological Sciences, University of Notre Dame, Indiana 46556, USA
(Received 16 December 2013; published 19 May 2014)

Passing a fluid through a grid is a well-known mechanism used to study the properties of turbulence. Oscillating a horizontal grid vertically in a tank has also been used extensively and is considered to be a source of almost homogenous isotropic turbulence. When the oscillating grid is turned on a turbulent flow is induced. A front translates into the experimental tank, behind which the flow is highly turbulent. Long predicted that the growth of such a front would grow diffusively as the square root of time (i.e., $d \sim \sqrt{t}$) and Dickinson and Long presented experimental evidence for the diffusive result at a low mesh Reynolds number of 555. This paper revisits these experiments and attempts a set of two models for the advancing front in both square and round tanks. We do not observe significant differences between runs in square and round tanks. The experiments in water reach mesh Reynolds numbers of order 30 000. Using some data from superfluid helium experiments we are able to explore mesh Reynolds numbers to about 43 000. We find the power law for the advancing front decreases weakly with the mesh Reynolds number. Using a very long tank we find that the turbulent front stops completely at a certain depth and attempt a simple explanation for that behavior. We study the propagation of the turbulent front into tubes of different diameters inserted into the main tank. We show that these tubes exclude wavelengths much larger than the tube diameter. We explore the variation of the position of the steady-state boundary H on tube diameter D and find that $H = cD$ with $c \sim 2$. We suggest this may be explained by saturation of the energy-containing length scale ℓ_e. We also report on the effect of plugging up just one hole of the grid. Finally, we recall some earlier oscillating grid experiments in superfluid ^{4}He in the light of the present results.

DOI: 10.1103/PhysRevE.89.053016 PACS number(s): 47.27.Gs

I. INTRODUCTION

Rouse and Dodu [1] appear to be the first to use oscillating grids as a source of zero-mean-shear turbulence for studying turbulent mixing and dispersion in homogeneous, stratified, rotating, or two-phase fluids. Thompson and Turner [2] studied scales of velocity and length in the fluid near the mixing interface. Dickinson and Long [3] and Hopfinger *et al.* [4] have measured the speed of propagation of turbulent fronts generated by oscillating grids in homogeneous fluids with and without rotation. Ivey and Corcos [5] have used oscillating grids to study boundary mixing in stratified fluids.

Oscillating grids are considered to be a source of almost homogenous isotropic turbulence. Careful discussion of the methods needed to achieve this have been given by De Silva and Fernando [6] (which includes a thorough literature survey), Fernando and De Silva [7], and Voropayev and Fernando [8]. When the oscillating grid rig is turned on a turbulent flow is induced. A front translates into the experimental tank, behind which the flow is highly turbulent. Long [9] predicted that the growth of such a front would vary diffusively as the square root of time (i.e., $d \sim \sqrt{t}$). In this work, which attracted considerable interest, Long modeled the induced flow as a system of point source-sink doublets of opposite sign arranged regularly in the plane of the grid. However, this model flow is irrotational, which is clearly not true for a turbulent flow.

The present paper describes the apparatus for visual and photographic analysis of the experiments in water. This paper presents two simple models for describing the advance of the turbulent front after starting the grid into oscillation in both square and round tanks and for several mesh sizes. It is found that the advance of the front can be described by a power law but that the exponent in the long-time decay depends weakly on the mesh Reynolds number. An earlier power law immediately followed on starting the grid into oscillation is also reported and its transition to long-time decay is found to be quite sharp.

We pursue the propagation of the front into a much deeper tank, and we discover that the front does not continue traveling down but stops at a definite depth. We advance a simple explanation for this phenomenon. We also study the motion of the turbulent front in circular tubes inserted into the tank with a variety of diameters. We find the circular tubes behave as a *high-pass filter*, where the word *high* refers to eddy wave numbers. Eddies with wavelengths larger than the tube diameter are less able to enter. We also describe the effect of blocking a single mesh hole in an experiment in water. Finally, we discuss some oscillating grid experiments in superfluid ^{4}He in the light of the present results.

II. EXPERIMENTAL APPARATUS

The apparatus evolved steadily as experience was gathered. In the early stages of this investigation we took the view that since we were studying turbulence the apparatus need not be of especially precise design. We know now that every attempt to improve the design yielded better results.

*rjd@uoregon.edu

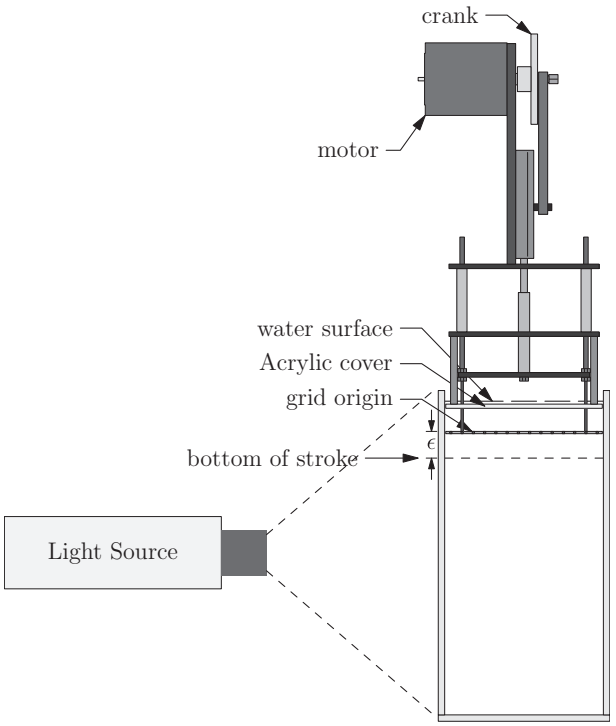

FIG. 1. Sketch of the experimental apparatus with the drive used in the early stages of this investigation. This tank had height $H = 36$ cm and width $W = 22$ cm. This apparatus was used for the data in Tables III–V and Figs. 9–12, and 14.

A. The tanks

Three square tanks of heights $H = 36$, 46, and 122 cm were constructed from sheets of 0.953-cm thickness acrylic, solvent welded. A bead of silicone guarded against occasional water leaks. Each tank had an inside width of $W = 22$ cm. We constructed one tank of cylindrical shape with diameter 30 cm. Results with the cylindrical design appeared generally consistent with the square design and are not reported here. The grid is usually placed 6.5 cm below the surface of the water. After a data run we waited some time to ensure equilibrium. We found that evaporation from the free surface drove weak convective rolls at the top of the tank. Placing a loosely fitting Plexiglas plate between the surface and the grid eliminated this problem.

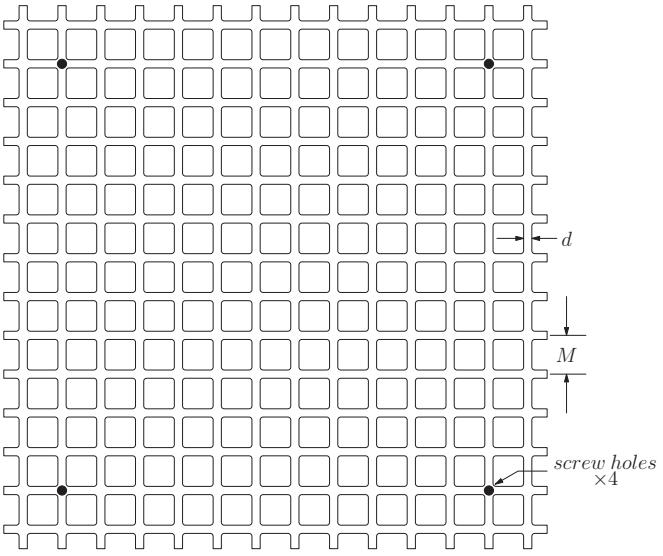

FIG. 2. Sketch of the grid design: $M = 1.59$ cm and $d = 0.318$ cm. The screw holes are for the four support rods.

B. The grids

The design of our system is illustrated in Figs. 1, 2, and 3. The oscillation takes place at a frequency f (circular frequency $\omega = 2\pi f$). The drive system has a stroke s, which is the distance the grid moves from bottom to top. The amplitude of the oscillation is $\epsilon = \frac{S}{2}$. Oscillating bars are governed by the Keuligan-Carpenter number N_{KC} and the Stokes number

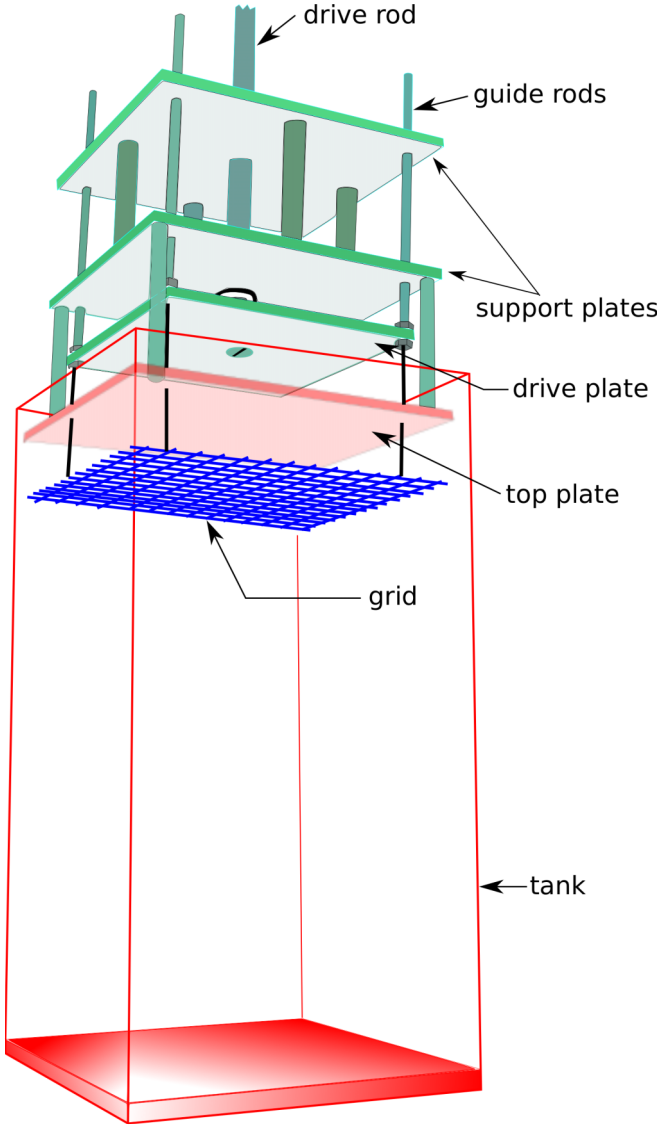

FIG. 3. (Color online) Sketch of the improved apparatus. Here the stepper motor and wheel are replaced by a linear motor (not shown). This apparatus was used for the pictures and data in Figs. 4, 5, 6, and 15.

TABLE I. N_{KC} numbers for the 1.59-cm mesh grid.

S (cm)	N_{KC}
1	11.5
2	20.9
3	31.4
4	41.9
5	52.4
6	62.8
7	73.3
8	83.8

St. For reference, these numbers for the grid bars are given in Tables I and II. The definitions are

$$N_{KC} = \frac{2\pi\epsilon}{d}, \tag{1}$$

$$St = \frac{fd^2}{\nu}, \tag{2}$$

where d is the thickness of the bars as shown in Fig. 2 and ν is the kinematic viscosity of the fluid.

The characteristic velocity of the grid is $U_o = \omega\varepsilon$, and the mesh Reynolds number is

$$Re_M = \frac{U_o M}{\nu}, \tag{3}$$

where M is defined as the distance from the center of one bar to the center of the next. Our best results (good reproducibility, relatively stable turbulent front) were obtained with the $M =$ 1.59 cm, $d = 0.318$ cm mesh as shown in Fig. 2.

The grid edges end in half a mesh in order to reduce the shear at the walls. The optimum grid design is described by De Silva and Fernando [6] as follows: "...to obtain nearly isotropic turbulence with zero-mean flow, certain design conditions have to be satisfied: the grid should have a solidity less than 40%, the oscillation frequency should be less than 7 Hz, the end conditions of the grid should be selected to yield low Reynolds stress gradients and measurements should be taken 2–3 mesh sizes away." The spacing between the ends of the grid tines and the tank wall is quite small, on the order of 0.025 cm. The half mesh spacing influenced the generation of large-scale motion in the tank: Typically the turbulent front will become unstable and speed down one side of the tank, a larger gap resulting in more unwanted motion. Also, unequal gaps on opposite sides resulted in greater large-scale motion. Towards the end of this investigation we used a high-precision grid of the same dimensions, machined by a numerically controlled mill. It is illustrated in Fig. 2. It is very important that the support rods for the grid are no larger than d. If they are not hidden by the grid, they will generate their own turbulent flow.

TABLE II. Stokes numbers for the 1.59-cm mesh grid.

f (Hz)	St
5	45
6	54
7	63
8	72
9	81
10	90

C. The motor drive

The grid support rods are connected as shown in Fig. 1 to a stepper motor with a torque of 2.8 N m turning a wheel with five holes drilled at various radii to provide a four-bar linkage to the grid providing variable frequency of oscillation and strokes s ranging from 1 to 5 cm. The frequency of the drive can be varied and ranged between 0.5 and 6 Hz.

Recently, we have replaced the stepper motor with a Copley Controls model STA2510S-104-S-S03X linear motor capable of 780 N of peak thrust. The grid supports are directly attached to the magnet rods of the motors, eliminating mechanical backlash. Also, the motors are brushless and ironless, resulting in smoother motion due to minimal motor cogging. The motors provide stroke lengths s anywhere between 0 and 10 cm.

The motor is driven by a Copley model XSL-230-18 Xenus indexer and amplifiers. Since the motors are brushless, electronic commutation is provided by the Xenus amplifier via linear Hall-effect sensors mounted on the forcer assembly. These same sensors also provide positional feedback. The basic resolution of the motors is 12.5 μm. The Xenus amplifiers are an entirely digital system, allowing ready reprogramming of the feedback loop coefficients, and they also internally generate the motion trajectory based on variables sent via an RS-232 link.

We found it advisable to attach the grid apparatus to a heavy platform supported by a concrete pillar to minimize vibration.

D. Visualization, lighting of the flow, and protocol

We found the problem of visualization of the flow of crucial importance to this experiment. Our first thought was to use the Baker thymol blue technique for visualization. This proved to give attractive pictures, but was of little use in tracking the turbulent front in practice. We finally used Kalliroscope to study the turbulent motions in water. Kalliroscope is a commercial product first described scientifically in a paper by Matisse and Gorman [10]. Exactly what is shown by light reflection from these anisotropic fish scale particles is still not entirely clear, although an analytical study by Savas [11] suggests that the flakes align themselves with stream surfaces with rapid turnovers and further notes that it is a useful technique for determining certain flow patterns. These scales align with the direction of shear and, when illuminated by a light sheet, give a good contrast between turbulent and nonturbulent regions. A discussion by Gauthier, Gondret, and Rabaud [12] is very useful in this respect: In particular, they show that the observed light cannot be used to reconstruct the velocity field. However, they do show that Kalliroscope can be used specifically to visualize vortical flow structures by comparing numerical predictions to experimental observations in Taylor-Couette flow.

Different lighting methods were tested for visualization. Shining white light through the whole tank caused visualization of all movement, which blocked the view of the turbulent front spreading down roughly at the center of the tank. We finally adopted a vertically collimated slit of light (1.5 cm

wide) from a slide projector shone through the center of the tank from left to right. On setting up the apparatus the length of the rod connected to the grid was adjusted so the grid position at the bottom of the stroke was 6.5 cm below the top cover. Since turbulence was measured from the bottom of the stroke, the stroke s, divided by 2 and subtracted from the 6.5-cm mark would give the mean position of the grid. We took the view that the origin of the turbulence was at the bottom of the stroke. Correcting to the mean position of the stroke did not affect the results in any significant way.

Distances from the grid were measured and marked with tape on two sides of the tank to avoid parallax. The grid would begin its oscillations (always from its lowest position), creating turbulence which would be revealed by light scattering from Kalliroscope flakes. The boundary between vortical and quiescent fluid was sharp and easy to observe. When the turbulent front reached a given tape mark, the time could be recorded electronically. Thus we could make a complete record of the propagation of the front down the tank in a single run. This efficiency allowed us to complete hundreds of runs in a reasonable period of time.

E. Photography of the front

Recently, we have implemented a machine vision camera situated approximately 130 cm in front of the tank. To calibrate the camera images, a metal scale is taped onto the face of the tank and photographed beforehand. The rest position of the grid is about 8 cm from the top of the tank. The grid oscillates about this point. When the grid oscillation begins, a sequence of photographs are taken at a fixed frame rate.

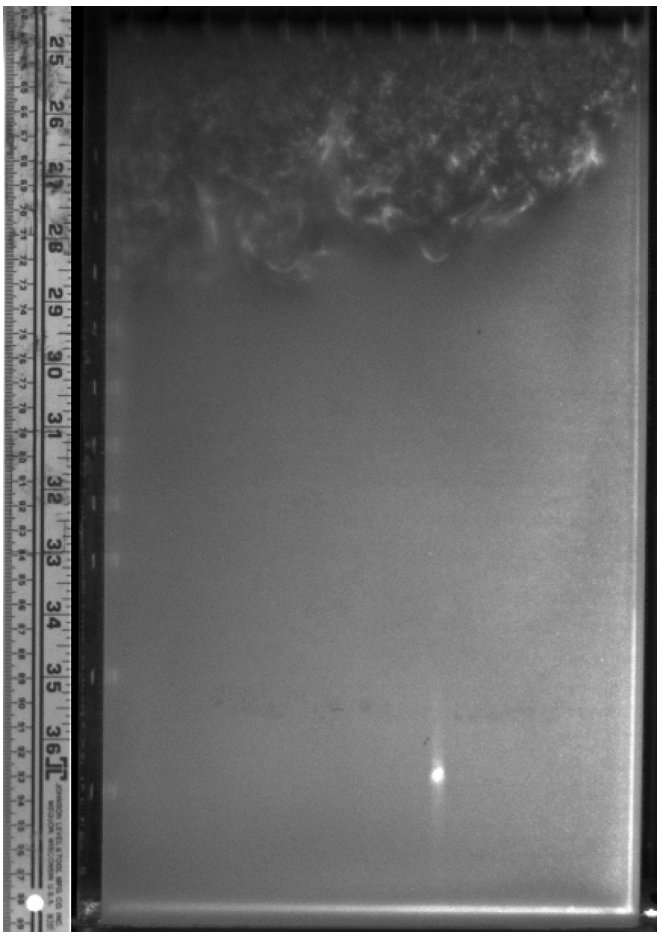

FIG. 4. Photograph of a turbulent front descending toward the bottom of the tank.

The position of the bottom of the turbulence field is measured off each photograph in the sequence using standard software tools [13]. Refer to Fig. 4 for a sample photograph. Note the photo of the metal scale is overlaid on the image to facilitate the measurement. The machine vision camera timestamps each photograph from a 100-MHz clock oscillator, allowing 10-ns timing precision. The result of this process is a list of position verses time data points which are plotted on a log-log scale using a standard plotting tool (gnuplot.info). Figure 5 shows an example of a plot of the advancing front displaying two power laws.

Repeating several experiments over a considerable range of variables presented in the tables in Sec. III, we found very similar results with the photographs.

III. EXPERIMENTAL RESULTS

A. The spreading of the turbulent front

The raw data from our experiment consisted of measurements of the position of the turbulent front in the center of the tank as a function of elapsed time. Long [9], on the basis of a theoretical analysis, proposed that the distance D traveled by the front in time t is given by

$$D = D_o + Kt^n, \tag{4}$$

where $n = 0.5$. Data analyzed by Dickinson and Long [3] gave experimental values of n close to 0.5. We attempted to apply the methods described by Dickinson and Long to our data. In particular, the location of the *artificial origin* of the turbulence D_o was found by fitting a power law $n = 0.5$ to the data to locate D_o, adding D_o to the data set, and then finding the value of n which gave the best fit to the combined data. On carrying

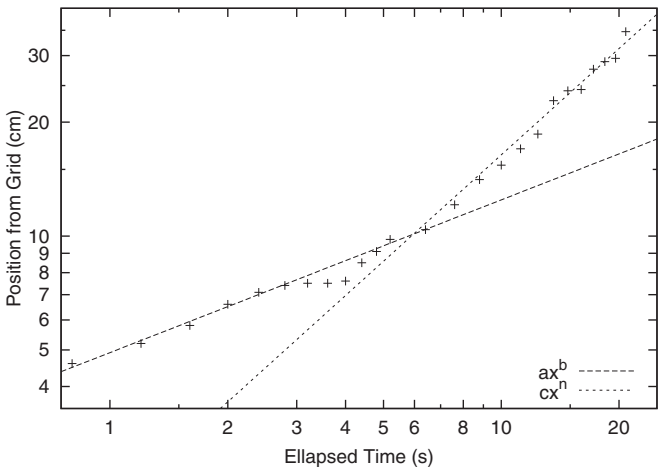

FIG. 5. Plot of photographic results showing two distinct powers with the change at approximately 10 cm (6.3 M) below the grid, at its lowest descent. The respective power laws are $b = 0.23$ and $n = 0.80$. The grid was oscillated with a frequency 5.00 Hz and amplitude 2.5 cm, providing a mesh Reynolds number of 12 500.

TABLE III. Data fitted to $D = D_o + Kt^n$ for the square tank. Notes: Each *set* consisted of the average of 10 trials with the results for the times at each position averaged together. Thus 3 represents 30 trials and 10 represent 100 trials. χ^2 is the usual statistical measure of goodness of fit.

M (cm)	f (Hz)	S (cm)	n	K	D_o (cm)	χ^2	sets
0.36	5.0	2.0	0.42	9.028	−7.70	0.157	3
0.36	5.0	5.0	0.35	24.20	−20.15	0.146	1
0.51	5.0	2.0	0.66	4.73	−3.34	0.059	3
0.51	5.0	5.0	0.57	13.71	−9.20	0.105	1
0.85	5.0	2.0	0.53	7.29	−7.05	0.022	3
0.85	5.0	5.0	0.66	12.93	−8.31	0.101	1
1.59	2.5	2.0	0.47	6.65	−6.59	0.120	10
1.59	3.75	2.0	0.62	4.73	−2.78	0.040	1
1.59	5.0	1.0	0.51	3.76	−3.40	0.018	10
1.59	5.0	2.0	0.45	10.8	−8.94	0.195	10
1.59	5.0	4.0	0.19	39.8	−36.1	0.108	10
1.59	5.0	5.0	0.24	35.8	−31.14	0.128	1
1.59	6.25	1.0	0.48	4.66	−4.02	0.045	1
1.59	6.25	2.0	0.59	7.60	−4.97	0.126	1
1.59	6.25	4.0	0.39	21.12	−17.37	0.071	1
1.59	6.25	5.0	0.24	40.71	−35.31	0.183	1
1.59	7.5	2.0	0.38	18.1	−16.20	0.191	10

this out we, too, found a power law near 0.5. However, using a power law of 0.4 to find D_o gave a fit with n near 0.4, and using a power law of 0.6 to find D_o gave a fit with n near 0.6. We concluded that this method was not suitable for our data.

The safest procedure, we believe, is to simply fit the data set directly to (4) and record the best fit values of K, n, and D_o. This has been carried out in Table III for the square tank. We have a complete set of experiments in round tanks, but the data did not substantially differ from square tanks and is omitted here.

Analysis with Eq. (4) showed that the artificial origin of the turbulence is located above the grid and can be many mesh lengths long. We therefore tried another simple model,

$$D = K(t - t_o)^n, \tag{5}$$

with $t > t_o$. The results of this analysis are shown in Table IV for the square tank. As can be seen (5) gives a much more reasonable result, with t_o of order 1 s, compared with a run duration 10 to 60 s. Indeed, we did two more analyses taking t_o to be 1 s and its average to be 1.3 s. This was an attempt to reduce the number of variables being found by the fitting routine. We do not reproduce these analyses here, for they did not appear to have any obvious advantage over the fits shown in Tables IV and V.

We also display in Table V the mesh Reynolds number defined in Eq. (3). Examination of some data concentrated in the first 10 cm or so revealed that the data in this range are simply linear in time. In order to explore this further we omitted data in the first 10 cm and reanalyzed the data as shown in Table V for the square tank.

Comparison of the χ^2 values between Tables IV and V demonstrate that a great improvement in the fit is obtained in this way. We conclude that something different is going on in the first few seconds of the experiment, perhaps the jets being produced by the grid take some time to organize themselves into a more homogeneous type of turbulence, which is what we saw in earlier investigations. A paper by Voropayev and Fernando [8] describes the evolution of the flow from the multipolar flow in each hole in the mesh to a distance down the tank where the jets from all the holes interact and start to make a turbulent flow. The authors cite Hinze [14] as the source of the transition at about $20M$. We have been able to shed some light on this process by recording the flow photographically.

We show some results in Fig. 5 in which the front moves down the tank a distance ~10 cm in about 4 s and has a power law $f(x) = ax^b$ with $b = 0.23$ followed by a distinct change in power law $f(x) = cx^n$ with $n = 0.80$. This change occurs at a distance 10 cm or $10/M = 6.3M$.

TABLE IV. Data fitted to $D = K(t - t_o)^n$ for the square tank.

M (cm)	f (Hz)	S (cm)	n	K	t_o (s)	χ^2	Sets
0.36	5.0	2.0	0.52	5.26	1.43	0.074	3
0.36	5.0	5.0	0.53	10.58	0.96	0.084	1
0.51	5.0	2.0	0.70	3.88	0.97	0.044	3
0.51	5.0	5.0	0.66	9.77	0.76	0.074	1
0.85	5.0	2.0	0.62	4.62	1.47	0.006	3
0.85	5.0	5.0	0.78	9.16	0.57	0.158	1
1.59	2.5	2.0	0.57	3.90	1.70	0.196	10
1.59	3.75	2.0	0.67	3.74	0.66	0.057	1
1.59	5.0	1.0	0.57	2.71	1.85	0.037	10
1.59	5.0	2.0	0.58	5.99	1.02	0.311	10
1.59	5.0	4.0	0.45	9.46	0.94	0.441	10
1.59	5.0	5.0	0.49	10.95	0.90	0.212	1
1.59	6.25	1.0	0.48	4.22	4.12	0.123	1
1.59	6.25	2.0	0.68	5.41	0.65	0.172	1
1.59	6.25	4.0	0.62	9.06	0.73	0.215	1
1.59	6.25	5.0	0.50	11.86	0.83	0.323	1
1.59	7.5	2.0	0.57	7.76	1.05	0.358	10

TABLE V. Data fitted to $D = K(t - t_o)^n$ for the square tank omitting data below 10 cm.

M (cm)	f (Hz)	S (cm)	n	K	t_o (s)	χ^2	Sets	Re_M
0.36	5.0	2.0	0.56	4.49	0.51	0.026	3	2300
0.36	5.0	5.0	0.48	11.84	1.22	0.0008	1	5700
0.51	5.0	2.0	0.77	3.10	0.05	0.0005	3	3200
0.51	5.0	5.0	0.59	11.29	1.05	0.022	1	8000
0.85	5.0	2.0	0.64	4.42	1.28	0.006	3	5300
0.85	5.0	5.0	0.65	11.68	0.95	0.035	1	13 400
1.59	2.5	2.0	0.50	5.14	3.66	0.036	10	5000
1.59	3.75	2.0	0.62	4.45	1.41	0.054	1	7500
1.59	5.0	1.0	0.53	3.15	3.57	0.008	10	5000
1.59	5.0	2.0	0.49	7.80	2.08	0.085	10	10 000
1.59	5.0	4.0	0.39	11.15	1.52	0.141	10	20 000
1.59	5.0	5.0	0.43	12.46	1.24	0.095	1	25 000
1.59	6.25	1.0	0.51	3.74	3.11	0.027	1	6200
1.59	6.25	2.0	0.57	7.39	1.62	0.105	1	12 500
1.59	6.25	4.0	0.54	10.79	1.09	0.105	1	25 000
1.59	6.25	5.0	0.42	14.07	1.21	0.029	1	31 200
1.59	7.5	2.0	0.48	9.77	1.75	0.114	10	15 000

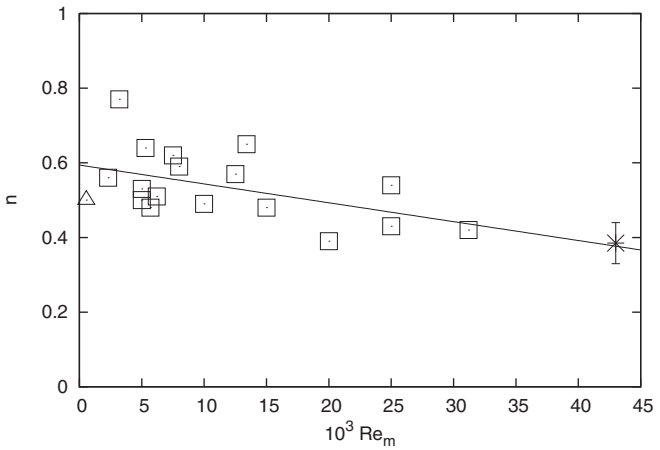

FIG. 6. Results for the power exponent n in Eq. (2) as a function of mesh Reynolds number from Table V in a square tank. The highest mesh Reynolds number point is taken from Smith's thesis [15] using liquid helium and the range of possible fits is given by the vertical bar. The experiments of Dickinson and Long [3] were at a mesh Reynolds number of 555 and are shown as a triangle. The trend line is given by $n = 0.594 - 0.005\,05 \times \mathrm{Re}_M$.

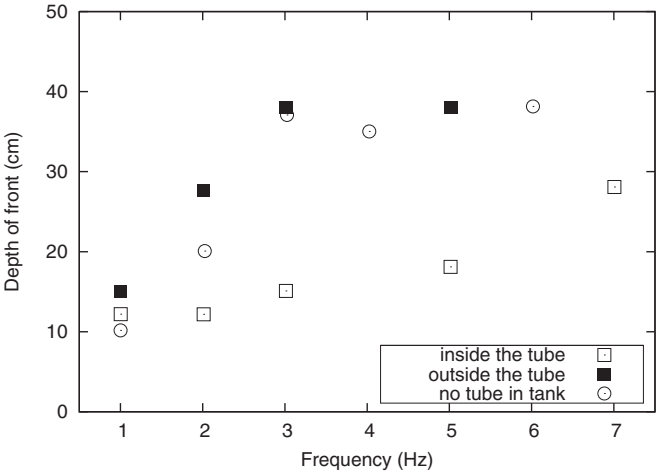

FIG. 7. Depth of the turbulent front in steady state in an oscillating grid experiment. The tube used in this experiment was 10 cm in diameter. This experiment shows that the presence of the tube did not disturb the turbulence in the main tank.

B. Results for the long-time power law as a function of mesh Reynolds number

We were unable to reproduce the results of Dickenson and Long [3] whereby the turbulent front spreads diffusively. Instead we find the power law described by n is a slow function of mesh Reynolds number over a great range of Reynolds numbers as shown in Fig. 6.

The large scatter seen in Fig. 6 reflects the fact that the propagating front in this type of experiment is often very unstable. The front tends to move to one side of the tank and plunge rapidly to the bottom. This behavior is perhaps the greatest limitation to this type of experiment. The highest mesh Reynolds number point is described in Sec. VII B.

IV. STATIONARY TURBULENT FRONTS IN SMALLER DIAMETER TUBES

We report on observations of the steady-state turbulent boundary in an oscillating grid experiment. We find that in a sufficiently deep tank the oscillating grid does not completely fill the tank with turbulence, even after long times. Instead, there is a boundary between turbulent and nonturbulent regions at a definite distance from the oscillating grid. We explore the variation of the position of the steady-state boundary H on tube diameter D and find that $H = cD$ with $c \sim 2$.

To observe the behavior of turbulence in different size containers, we hang Plexiglas tubes of various diameters D ($0.6\ \mathrm{cm} < D < 17\ \mathrm{cm}$) in the main tank. The tubes have a wall thickness of 0.3 cm. They are supported by a simple rigid harness that spans the width of the tank well below the region where turbulence exists in the tubes. The harness is suspended by strings that clip onto the top edges of the walls of the tank. With this system, we are able to position the tube anywhere in the tank and at any height. We usually make our measurements with the tube near the center of the tank. The tubes are typically 50 cm long, with the top end open and the bottom end plugged.

To illustrate the observations, Fig. 7 shows the steady-state turbulent boundary as a function of oscillation frequency for the empty tank and for a 10-cm-diameter tube placed in the tank. The tube was placed just off center. We measure the depth simply by estimating by eye the edge of the turbulent region and measuring with a ruler the distance between this point and the midpoint of the grid stroke. The measurement is made difficult by the fact that the boundary is undulating across the width of the tank, reflecting the wide range of eddy sizes that make up the turbulence. The boundary advances and retreats in the tube over time suggesting intermittency. We attempt to identify the average position of the boundary. The measurements are made after waiting 10–15 min after turning on the grid motor to ensure that the boundary is no longer advancing. We have compared the depths measured after waiting 15 min to depths measured after waiting 1 h and found no difference within experimental error. To investigate this phenomenon further we devised the measurement shown schematically in Fig. 8.

A tube of diameter D hung a distance L below the grid will measure a penetration depth h, which is the distance between the mouth of the tube and the boundary between turbulent and nonturbulent regions in the tube. We record h for a variety of values of L and calculate the total depth of the boundary $H = L + h$. If the distance that the turbulence propagates in the tube depends in some way on the interaction with the tube, then measurements made at different values of L will not recover the same H. For example, if the turbulent energy in the tube were primarily generated at the tube mouth, perhaps by vorticity generation at the edges, then one would expect the penetration depth h to be a constant, independent of L.

We used hanging heights of $L = 4$ to 10 cm. The grid was oscillated at 1, 3, and 5 Hz with a stroke of 1.5 cm. As expected, the penetration increases with frequency and with closeness to the grid. Figures 9–12 show the total depth H calculated by adding h to L. For each frequency a reasonably constant value of H is measured. A crude measure of the collapse is given by the dimensionless spread $\Delta H/H \approx 0.1$ in Fig. 9 to

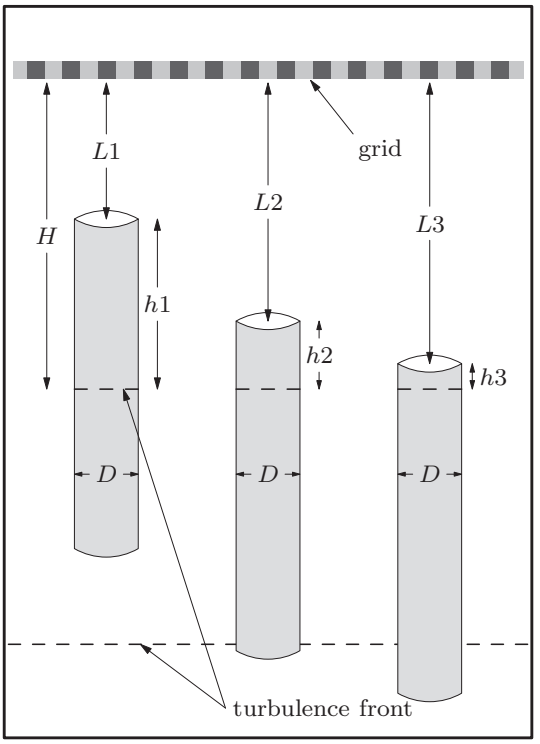

FIG. 8. Schematic illustration of the measurement of the turbulence front in a tube hung in the tank at different depths L.

$\Delta H/H \approx 1$ in the smallest tube in Fig. 12. While the errors are rather large ($\sim\pm 10\%$) and the data do not collapse perfectly, there does not seem to be any systematic variation with L.

Figure 12 shows rather poor collapse of the H data and a systematic variation with L, indicating that the tube is affecting the measurement. We found that for tube diameters larger than 3 cm there is generally good collapse of the data and the H measurement was meaningful. For smaller tube diameters the measurement was not meaningful. It is known that closer than 2–3 mesh lengths to the grid the flow is

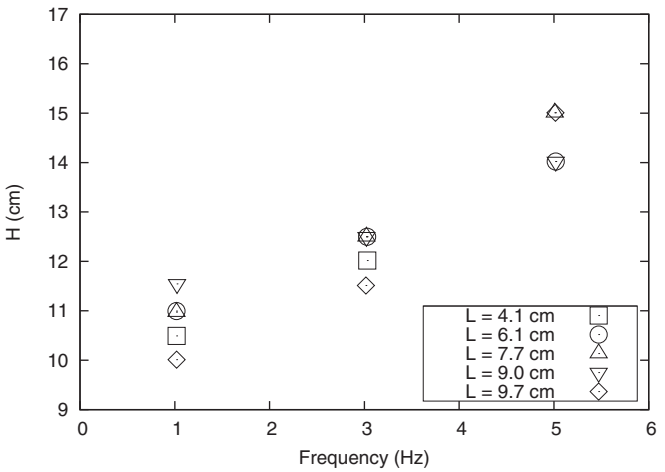

FIG. 9. Depth of steady-state turbulent front in a tube 5.7 cm inner diameter for various frequencies. The collapse of H is quite good for this larger tube. Here $\Delta H/H \approx 0.1$.

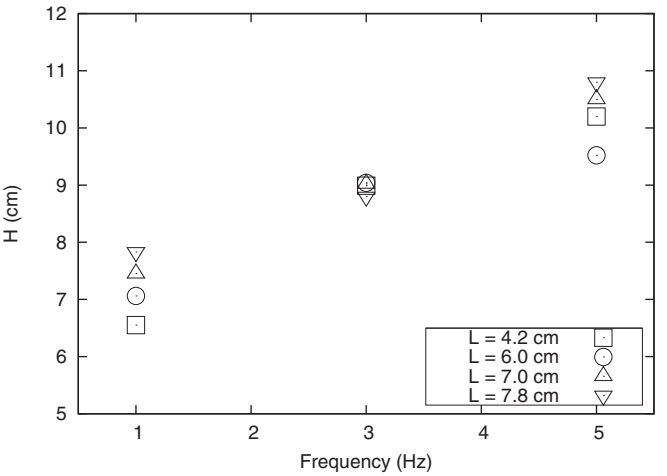

FIG. 10. Depth of the steady-state turbulent front in a tube of 3.17-cm inner diameter for various frequencies. The collapse is still good for this diameter tube, $\Delta H/H \approx 0.2$.

dominated by jets produced by the grid [14]. Only further from the grid do the jets merge to form homogeneous turbulence. Therefore, we should not expect reasonable results closer than $\sim$5 cm to the grid [14]. In fact our own measurements as seen in Fig. 5 suggest a distance $\sim$10 cm might be more appropriate.

V. ENERGY SPECTRUM: HIGH-PASS FILTER

It is not surprising that the turbulent front reaches a steady-state depth. As the turbulence travels away from the generation region next to the grid, the turbulent energy decays via the energy cascade and viscous dissipation. At some depth, the turbulent energy should decay to zero and the front can no longer propagate. The smaller the diameter of the tubes the less we expect the front to descend as was observed in the experiments. The reason for this is that smaller diameters exclude the turbulent energy at larger scales. Essentially, the tube acts as a filter, excluding eddies larger than

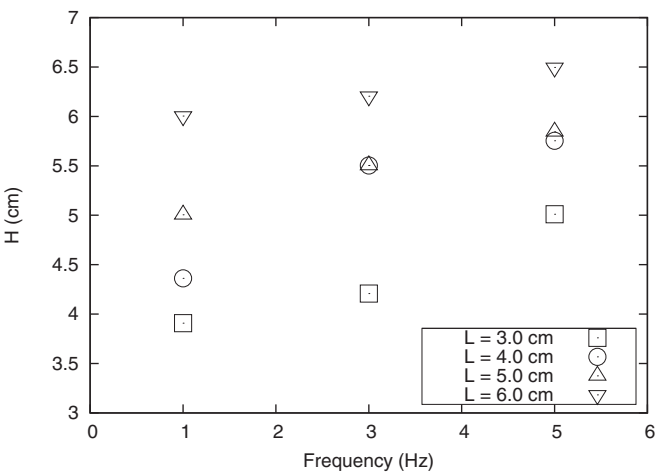

FIG. 11. Depth of the steady-state turbulent front in a tube of 1.6-cm inner diameter for various frequencies. Here $\Delta H/H \approx 0.8$.

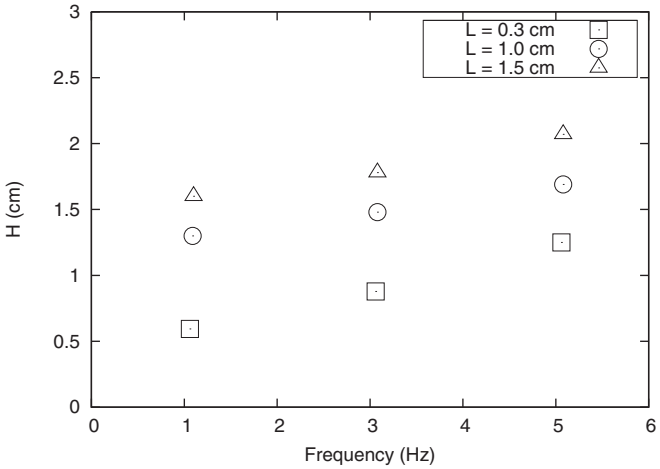

FIG. 12. Depth of the steady-state turbulent front in a tube of 0.6-cm inner diameter for various frequencies. The data do not collapse for this small diameter tube, $\Delta H/H \approx 1$.

the tube diameter. The decay of turbulence becomes faster when the energy containing length scale ℓ_e of the turbulence becomes comparable to the length scale of the container [16]. Therefore, in the oscillating grid experiment we expect the energy containing length scale to be comparable to that of the tank or tube, after which accelerated decay of turbulence will occur,

$$\ell_e = \left(\frac{3\pi}{4}\right)\frac{\int_{\frac{2\pi}{D}}^{\infty} k^{-1}\, E(k)\, dk}{\int_{\frac{2\pi}{D}}^{\infty} E(k)\, dk}. \tag{6}$$

We have ignored viscous effects in the above equation by leaving the upper limit of integration as ∞. We define the energy containing wave number as $k_e = 2\pi/\ell_e$. For small wave numbers ($k \leqslant k_e$) we use $E(k) = Ak^2$ and for the large wave numbers ($k \geqslant k_e$) we use the Kolmogorov law $E(k) = C\varepsilon^{2/3}k^{-5/3}$. This gives

$$\ell_e = \left(\frac{3\pi}{4}\right)\frac{\frac{11}{10}k_e^2 - \frac{1}{2}\left(\frac{2\pi}{D}\right)^2}{\frac{11}{6}k_e^3 - \frac{1}{3}\left(\frac{2\pi}{D}\right)^3}. \tag{7}$$

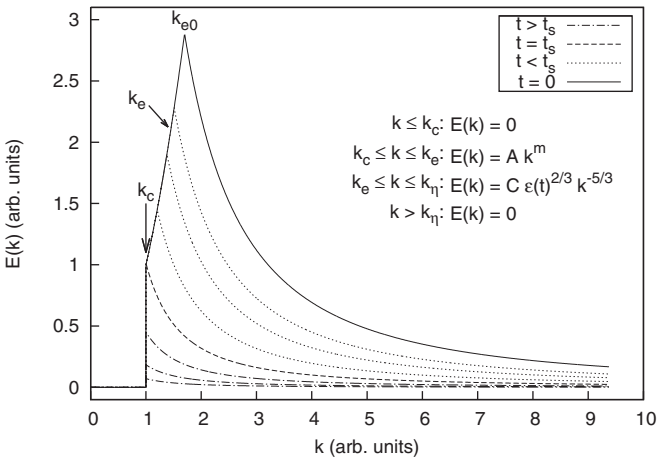

FIG. 13. Energy spectrum in a finite channel after Stalp *et al.* [16].

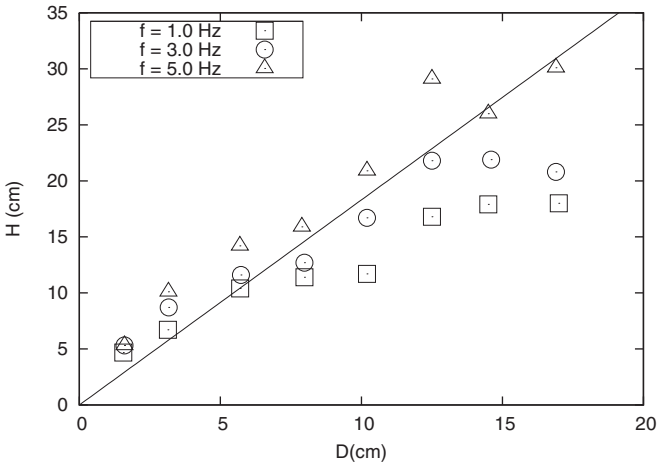

FIG. 14. Measurement of H as a function of tube diameter for three oscillation frequencies. The solid line represents Eq. (8).

We can determine the depth at which the energy containing length scale is the same as the characteristic length scale of the container D. This depth is given by the sole real root of the cubic equation above,

$$\ell_e = \frac{2\pi D}{3.429} = 1.83D, \tag{8}$$

and in this experiment l_e is identified with H and D is taken as the diameter of the tube (Fig. 13).

Once the turbulence reaches this depth the energy decays rapidly. If the faster decay is sufficiently rapid we expect the turbulent front to be close to this depth. In Fig. 14 we compare this depth to the depth of the steady-state turbulent front from the experiments. Overall the data appear consistent with this hypothesis, except for the largest-diameter tubes at the smaller forcing frequencies.

VI. ANOMALOUS JET FORMATION

During the initial setup of the experiments we noticed the formation of a jetlike structure that propagated down well beyond the turbulent front described in the previous two subsections of this paper. Upon further investigation we noticed that this structure was formed from a region where the mesh did not maintain the same structure as elsewhere. By plugging up one of the holes in the mesh we saw that such a jet was formed, as illustrated in Fig. 15. This fast-moving plume overtakes the main turbulent front and one possible explanation is that it is a vortex street such as we reported coming from an oscillating pendulum in Ref. [17], except that the street is turbulent. Reference [17] shows that the damping of a pendulum oscillating in water is influenced by the emission of vortex rings.

VII. GRID TURBULENCE EXPERIMENTS IN SUPERFLUID ^{4}He

A. Quantized vortex lines

Liquid ^{4}He above the λ transition (2.1768 K) is a perfectly classical fluid hydrodynamically and is called helium I. Below the λ transition helium II obeys a pair of equations: one for the normal *viscous* fluid having density ρ_n and velocity v_n and one

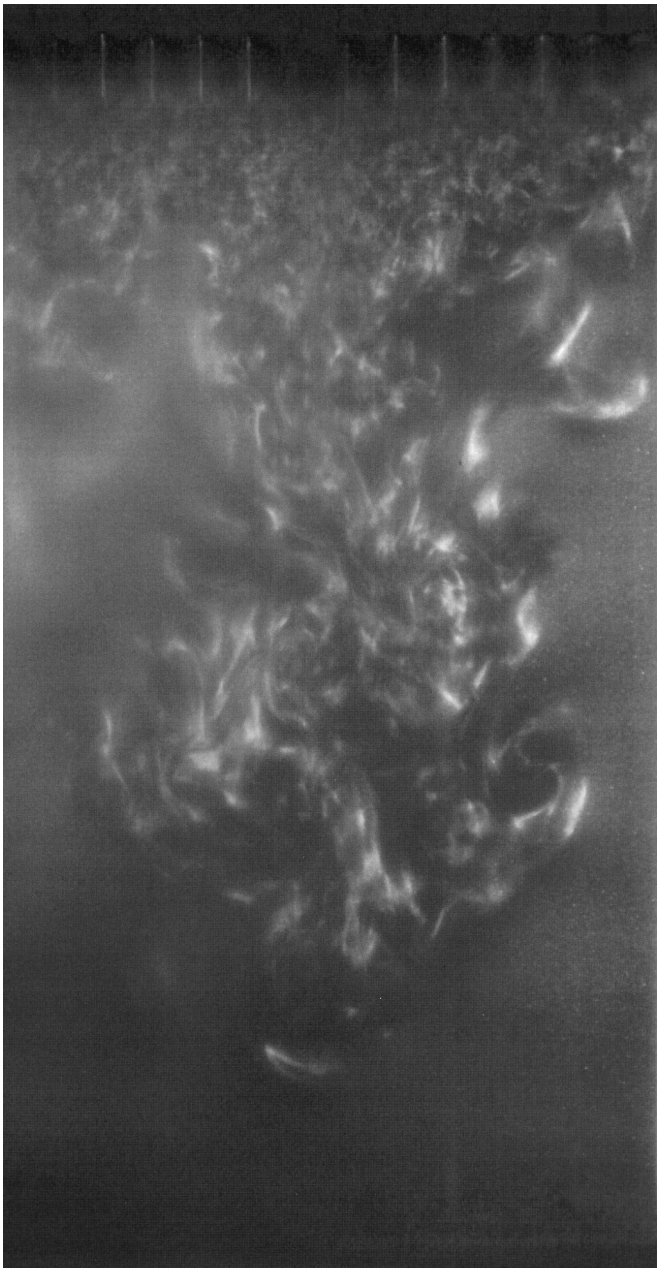

FIG. 15. Photograph of the fast-moving plume generated when the central hole in the grid is plugged and is much wider than the mesh size M. The rapid motion of this flow suggests that it might arise from a street of vortex rings such as we reported in Ref. [17], except that the rings are turbulent. The mesh used to generate this image is as described in Fig. 2. The top of this image shows a total width of $13M \approx 20.7$ cm.

for the superfluid, an absolutely *inviscid* fluid, having density ρ_s and velocity v_s. The total density ρ is the sum of the normal and superfluid densities which are separately strong functions of temperature. The equations of motion for the velocity fields depend on the entropy S of the fluid and the Kelvin temperature T. The equations of motion yield two forms of "sound," an ordinary wave having density fluctuations and another wave called "second sound" exhibiting entropy fluctuations. More detailed experiments at Leiden showed that under certain circumstances an extra term was needed to couple the velocity fields of the two fluids which was called "mutual friction." The underlying physics of mutual friction was investigated later by W. F. Vinen and H. E. Hall in Cambridge (see, for example, Ref. [18]).

When helium II is set into rotation at angular velocity Ω the superfluid cannot rotate in the classical sense because the superflow is irrotational in a simply connected region. Nevertheless, the entire fluid does rotate, seemingly classically, but the reason is that the superfluid generates a uniform array of quantized vortices each with circulation $\kappa = h/m$ where h is Plank's constant and m is the (bare) mass of the helium atom. The vorticity of the rotating superfluid is $\omega = 2\Omega$, the same as the vorticity in a classical fluid in a rotating container. While quantized vortices were suggested theoretically by Onsager and Feynman [19] no experimental evidence appeared until Vinen and Hall did their thesis work in Cambridge in the mid-1950s.

The pioneering experiments in the turbulent flow of helium II were carried out at Cambridge in helium II by W. F. Vinen and reported in a series of four papers which appeared in 1957 [20–23]. When turbulence is present, which Vinen induced using a heater at one end of a channel, quantized vortex lines are generated and can tangle together but remain quantized with circulation $\kappa = h/m$, where h is Planck's constant and m is the mass of the helium atom. It was only during this investigation that the role of quantized vortex lines was realized and experiments by Vinen and Hall provided insight into their behavior. The remarkable thing is that in a turbulent flow, in contrast to turbulence in ordinary fluids such as water and air, all vortices have the same size and same quantized circulation. This makes a major simplification in the study of turbulence. Unfortunately, when turbulence is present, the quantized vortices interact with the normal fluid. The only way to get around this problem is to take advantage of the fact that the normal fluid density decreases with temperature and seek to use the lowest temperatures available. For many years this study was called "superfluid turbulence," but on realization that if Planck's constant were zero, the field would not exist, and the name "quantum turbulence" is now in common use [24,25].

When turbulence is present in helium II in the form of a tangle of quantized vortex lines, second sound is attenuated, and by measuring the attenuation one can deduce the magnitude of the vorticity in the superfluid [18]. Vorticity in the superfluid couples the two velocity fields, and the two fluids act as one by mutual friction; indeed the kinematic viscosity above 1 K and at larger scales is approximately the viscosity divided by the total density.

Experiments with towed and oscillating grids in superfluid ^{4}He have been carried out for a number of years at the University of Oregon. In particular, Michael Smith presented a Ph.D. thesis in 1992 with observations on the vorticity of the superfluid induced by a towed grid and an oscillating grid [15]. Steven Stalp then took over the apparatus, presenting his thesis in 1998 [26]. Normally, we would be reluctant to compare data taken below the λ transition to experiments in water because the hydrodynamics of helium II require a two-fluid set of equations. However, Smith reports that his results are independent of temperature and viscosity, so as a guess we take the kinematic viscosity of liquid helium at 2.13 K

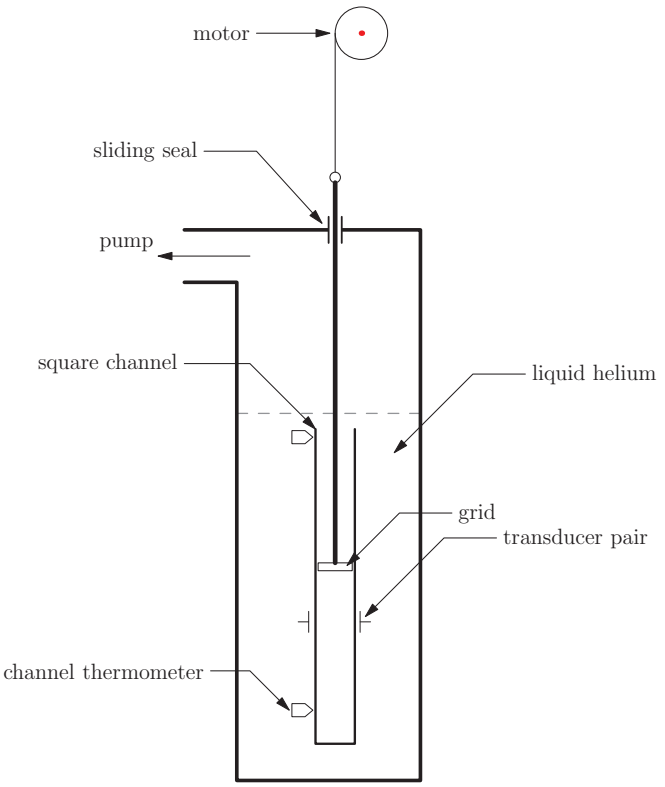

FIG. 16. (Color online) Sketch of the apparatus used by Smith to study towed grid experiments in helium II [15]. The second-sound transducers are directly across from each other: one generates second sound and one detects it. The thermometer was fed to an electronic temperature controller.

(his highest temperature), which is approximately $\nu = 1.38 \times 10^{-4}$ cm^2/s. Smith had $f = 3.75$ Hz, $M = 0.20$ cm, and $\varepsilon = 1.25$ cm, giving, finally, $n = 0.435$ at $\mathrm{Re}_M = 4.27 \times 10^4$.

Smith's apparatus is sketched in Fig. 16, and one of his grid designs is shown in Fig. 17.

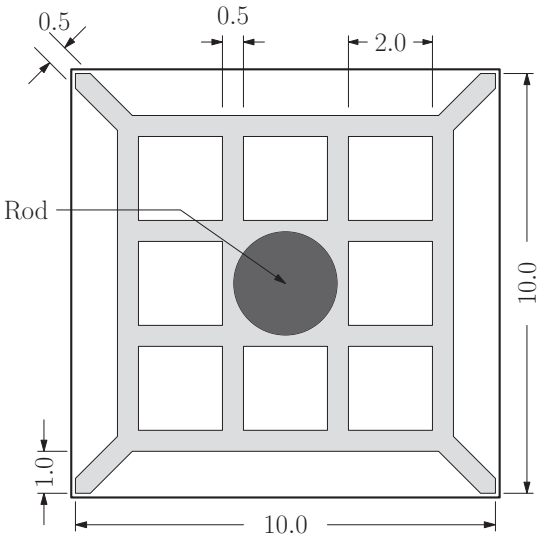

FIG. 17. Sketch of one of the sliding grid configurations used by Smith [15], where the dimension is millimeters.

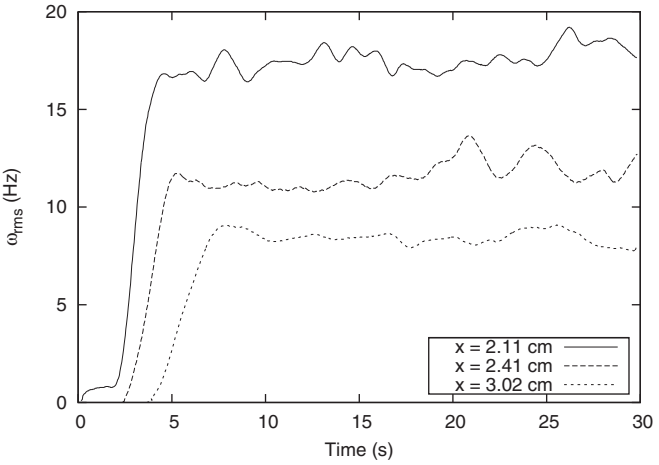

FIG. 18. Typical averaged signal for the oscillating grid. The three values of x illustrate the effects of varying x and the steady-state vorticity. Note that the sharp front does not look like a diffusive process [15].

The sliding grid apparatus has been described in detail in Smith's and Stalp's theses [15,26] and in other papers [27]. Briefly, the channel is a 1 cm × 1 cm brass channel, 40 cm long. The grid is actuated by a stepping motor mounted outside the cryostat. Most of the experiments were initiated by sweeping the grid the full length of the channel and monitoring the decay by attenuation of second sound, which can be interpreted as giving the vorticity averaged over about 1 cm^3. This averaging results in a quiet signal which can be followed over about 6 decades of vorticity.

B. Oscillating grid experiments in helium II

Once the first results with this apparatus were understood, it seemed sensible to try an oscillating grid. Our experiments could be conducted down to about 1.2 K. Oscillating grid experiments in the difficult range below 1 K, and indeed to

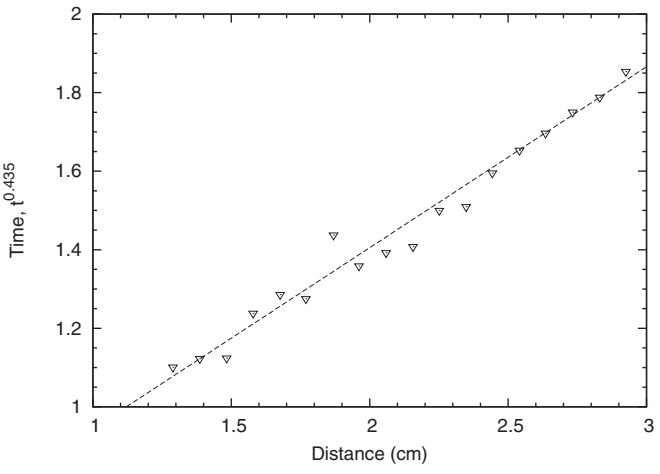

FIG. 19. Smith's data fitted to $x \sim t^n$ with the best fit yielding $n = 0.435$. But Smith also states that a fit to $n = 0.333$ looks just as good. The results were found to be independent of temperature, suggesting the two fluids are locked together [15].

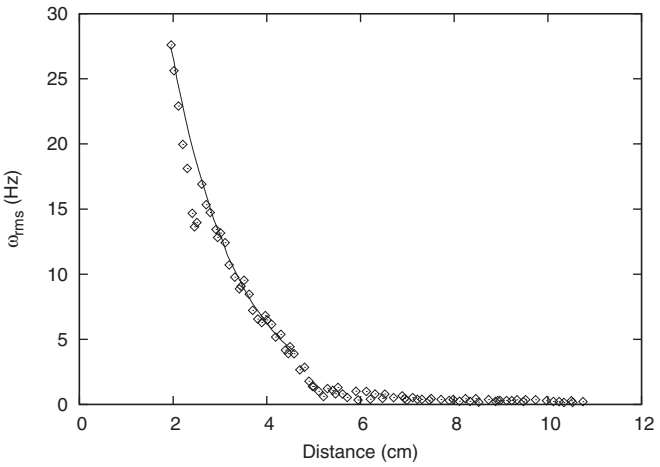

FIG. 20. Steady-state vorticity for the oscillating grid as a function of distance in helum II. The channel was 1 cm × 1 cm. The abscissa is the mean distance the second-sound tranducers are from the oscillating grid. For $\omega > 4$ Hz the solid line $\omega(x) = 113\exp(-\frac{x}{1.39})$ describes the data fairly well, but we do not understand the physical basis for this behavior [15].

millikelvin temperatures have been reported in a series of papers from McClintock's group at the University of Lancaster [28–31].

The oscillating grid was driven by a roughly triangular waveform. Results at three different distances from the grid to the transducers are shown in Fig. 18. The sharp leading edge of the received signal suggests a propagating pulse and not a diffusive process, as suggested by Long [9] for classical fluids. Taking the averaged vorticity as a function of x resulted in the data of Fig. 19. Like the experiments in Sec. III, the turbulent front ceases to spread after a finite distance (Fig. 20). However, the channel size is 1 cm, so the front is reaching about five channel widths instead of the one or two that we see in Fig. 9. At first we speculated that the central post in the grid seen in Fig. 17 might be sending a fast-moving plume such as we see in Fig. 15. However, if that were true we should see two fronts arriving at different times. There is no such phenomenon in the data of Fig. 18, so no definite conclusion can be reached at this time.

VIII. DISCUSSION

Turbulence generated by grids is now quite an old subject starting in the 1940s and continuing ever since. The newer study of quantum turbulence has greatly extended our knowledge of the subject. Turbulence decay experiments in helium II can be followed over six orders of magnitude of vorticity, providing information that would have needed a wind tunnel 1000 km long. Oscillating grid experiments described in this paper including one measurement in helium II have extended mesh Reynolds numbers from a few hundred to about 43 000. The long decay exponent is a weak function of mesh Reynolds number in contrast with the diffusive claim in Dickinson *et al.* [3] and Long [9].

ACKNOWLEDGMENTS

The information in this paper was greatly improved through the efforts of Chris Swanson and Stephen Hall. We are greatly indebted to W. F. Vinen for suggesting the sliding grid experiment in helium II. Nothing would have come of the superfluid helium experiments without the efforts of Michael Smith and Steven Stalp. We are indebted to K. Sreenivasan and L. Skrbek for reading the manuscript.

[1] H. Rouse and J. Dodu, La Houille Blanche **4**, 522 (1955).
[2] S. M. Thompson and J. S. Turner, J. Fluid Mech. **67**, 349 (1975).
[3] S. C. Dickinson and R. R. Long, Phys. Fluids **21**, 1698 (1978).
[4] E. J. Hopfinger, F. K. Browand, and Y. Gagne, J. Fluid Mech. **125**, 505 (1982).
[5] G. N. Ivey and G. M. Corcos, J. Fluid Mech. **121**, 1 (1982).
[6] I. P. D. DeSilva and H. J. S. Fernando, Phys. Fluids **6**, 2455 (1994).
[7] H. F. S. Fernando and I. P. D. DeSilva, Phys. Fluids A **5**, 1849 (1993).
[8] S. I. Voropayev and H. J. S. Fernando, Phys. Fluids **8**, 2435 (1996).
[9] R. R. Long, Phys. Fluids **21**, 1887 (1978).
[10] P. Matisse and M. Gorman, Phys. Fluids **27**, 759 (1984).
[11] Ö. Savas, J. Fluid Mech. **152**, 235 (1985).
[12] G. Gauthier, P. Gondret, and M. Rabaud, Phys. Fluids **10**, 2147 (1998).
[13] http://www.gimp.org.
[14] J. O. Hinze, *Turbulence*, 2nd ed. (McGraw-Hill, New York, 1975).
[15] M. R. Smith, Ph.D. thesis, University of Oregon, 1992.
[16] S. R. Stalp, L. Skrbek, and R. J. Donnelly, Phys. Rev. Lett. **82**, 4831 (1999).
[17] D. Bolster, R. E. Hershberger, and R. J. Donnelly, Phys. Rev. E **81**, 046317 (2010).
[18] R. J. Donnelly, *Experimental Superfluidity* (University of Chicago Press, Chicago, 1967).
[19] R. J. Donnelly, *Quantized Vortices in Helium II* (Cambridge University Press, Cambridge, 1991).
[20] W. F. Vinen, Proc. R. Soc. London A **240**, 114 (1957).
[21] W. F. Vinen, Proc. R. Soc. London A **240**, 128 (1957).
[22] W. F. Vinen, Proc. R. Soc. London A **242**, 493 (1957).
[23] W. F. Vinen, Proc. R. Soc. London A **243**, 400 (1958).
[24] R. J. Donnelly and C. E. Swanson, J. Fluid Mech. **173**, 387 (1986).
[25] W. F. Vinen and R. J. Donnelly, Phys. Today **60**, 43 (2007).
[26] S. R. Stalp,Ph.D. thesis, University of Oregon, 1998.
[27] M. R. Smith, R. J. Donnelly, N. Goldenfeld, and W. F. Vinen, Phys. Rev. Lett. **71**, 2583 (1993).
[28] S. I. Davis, P. C. Hendry, and P. V. E. McClintock, Physica B **280**, 43 (2000).
[29] H. A. Nichol, L. Skrbek, P. C. Hendry, and P. V. E. McClintock, Phys. Rev. E **70**, 056307 (2004).
[30] H. A. Nichol, L. Skrbek, P. C. Hendry, and P. V. E. McClintock, Phys. Rev. Lett. **92**, 244501 (2004).
[31] D. Charalambous, L. Skrbek, P. C. Hendry, P. V. E. McClintock, and W. F. Vinen, Phys. Rev. E **74**, 036307 (2006).